Arabian Journal of Chemistry (2022) **15**, 103946

King Saud University

Arabian Journal of Chemistry

www.ksu.edu.sa
www.sciencedirect.com

ORIGINAL ARTICLE

Activated carbon and its hybrid composites with manganese (IV) oxide as effectual electrode materials for high performance supercapacitor

Dibyashree Shrestha

Department of Chemistry, Patan Multiple Campus, Tribhuvan University, Patan Dhoka, Lalitpur 44613, Nepal

Received 2 December 2021; accepted 1 May 2022
Available online 11 May 2022

KEYWORDS

Activated carbon;
Aqueous electrolyte;
Manganese IV oxide;
Hybrid composite;
Supercapacitor

Abstract Waste wood-dust of *Dalbergia sisoo* (Sisau) is presented, as a novel, low-cost, renewable, and sustainable source of agro-waste for the production of a highly porous activated carbon electrodes (Ds-electrodes) for supercapacitor. Ds-electrode was initially tested as supercapacitor electrode, which showed a lesser specific capacitance of 104.4 Fg^{-1}. Therefore, hybrid-composite-electrodes (HCEs) were fabricated by adopting the nanostructured "manganese IV oxide (MnO_2)-activated carbon (Ds) composite" in various ratios as the core electrode materials. The HCEs was prepared via a simple facile mechanical mixing method and polyvinylidine fluoride (PVDF) polymeric solution was used as the electrode material binder. The experimental results showed that the 1:1 Ds: MnO_2 composite displayed highest specific capacitance of 300.2 Fg^{-1}, capacity retention of 96.3 % after 1000 cycles, 16.3 $WhKg^{-1}$ of specific energy density at power density of 148.2 WKg^{-1} and low equivalent series resistance (ESR) value of 0.41 Ω at equivalent (1:1, Ds:MnO_2) loading of MnO_2 to Ds. It is clear that the equivalent (1:1) concentration of MnO_2 has improved the capacitive performance of the composite via pseudocapacitance charge storage mechanism as well as the enhancement on the specific surface area of the electrode. However, further increasing of the MnO_2 content (1:2, Ds:MnO_2) in the electrode was found to distort the capacitive performances and deteriorate the specific surface area of the electrode, mainly due to the aggregation of the MnO_2 particles within the composite.

1. Introduction

In recent years, the excessive consumption of traditional energy sources such as coal, oil, and natural gas, have caused a global crisis and severe global climate which increasingly deteriorating ecological environment that endangers human survival (Sun et al., 2015; Seh et al., 2017). To cope with the growing demand and supply of energy storage, there is an immediate necessity of

E-mail address: shresthadibyashree@gmail.com
Peer review under responsibility of King Saud University.

Production and hosting by Elsevier

https://doi.org/10.1016/j.arabjc.2022.103946

development of new electrochemical energy storage (EES) devices which are renewable, efficient, reliable and cost-effective because of their advantages of providing high energy and high power density instantly (Ndiaye et al., 2018).

Among different kinds of EES devices, supercapacitors (SCs) have the characteristics of a long cycling life or capacity retention with greater capacitance than conventional capacitors/lithium-ion batteries (Yu et al., 2019), and have broad application prospects in many fields like in portable electronics, data back-up, hybrid electric vehicles, aerospace, and other fields owing to its simple structure, high power density, fast charging, and pollution-free effects in the production process (Dai et al., 2018).

Generally, SCs can be classified into two types: electric double layer capacitors (EDLCs) and pseudocapacitors (Lee et al., 2012; Yang and Park, 2018). The capacitance of EDLCs mainly depends on the adsorption of anions and cations on or near the electrode/electrolyte interface, which is mainly related to the surface area of the electrode materials. Porous carbon, such as activated carbon (Yaglikci et al., 2020; Huang et al., 2019), carbon nanotubes (Zhang et al., 2017; Liu et al., 2019), carbon nanofibers (Chang et al., 2019; Yang et al., 2019) and graphene (Ke and Wang, 2016; Li et al., 2016), is a commonly used electrode material for EDLCs. Porous carbon materials are the best suited material for achieving a high capacitance, since they combine high electric conductivity, chemical and physical stability (Zhu et al., 2016). Many carbons possess naturally occurring surface quinones (Selvakumar et al., 2010). However to increase their capacitance, the type and extending of quinone functionalization can be optimized by ''activated'' carbon, which increases surface area of carbon (Ren et al., 2016). This kind of carbon material has a high specific surface area and good conductivity, which can improve higher specific capacitance. Although graphene and carbon nanotubes have better conductivity and surface area than other carbons, activated carbons has become an ideal electrode material for EDLCs, and is used on a large scale for commercialized supercapacitors due to its easy processing and lower cost, adjustable surface area, relatively inert electrochemical properties, adjustable porosity and electrocatalytically active sites for reactions (Liang and Xin, 2015). However, relatively low capacitance, energy density (<10 Whkg^{-1}), power density and capacity retention (cyclic stability) are the major drawbacks of such carbon materials (Shrestha et al., 2019; Salinas-Torres et al., 2019; Brousse et al., 2006).

In order to solve these problems, there have been tremendous efforts on improving the performances of AC material by manipulating the pore characteristics and surface area (Gonzalez-Serrano et al., 2004; Xie et al., 2020). It has been found that physical activation leads to a more concentrated pore size distribution, while chemical activation can increase the bulk density and thus increase the adsorption capacity (Liang and Xin, 2015; Sing and Verma, 2015). In addition, there is a continued effort to combine the carbon material with metal oxide or a conductive polymer to enhance the capacitance performance through the synergistic effect of EDLC and the pseudocapacitors (Li et al., 2019). A composite of NiO with activated carbon was found to give a specific capacitance of 214.48 Fg^{-1} at 40 mAg^{-1} in a 1 M KOH aqueous solution (Cao et al., 2016). Similarly, addition of MnO_2 to activated carbon nanotube resulted in enhancing specific capacitance of 90.5 Fg^{-1} (Kim et al., 2013). Recently, there has been a focus on 2D metal carbides and nitrides (MXenes) as a very promising supercapacitor material (Sarkar et al., 2015; Lufrano and Staiti, 2010; Zequine et al., 2017; Cao et al., 2017).

From the above discussion, it is clear that the major research focus on supercapacitor electrode material is on obtaining high surface area activated carbon from renewable source. Wood dust material is one of the most economical and environmentally-friendly materials showing better electrochemical performance (Xie et al., 2018). More importantly, the effective use of bio-mass resources has become a hot topic because bio-mass resources are available in large quantities every year (Zhao et al., 2019). In our previous study (Shrestha, 2021), agro-waste of *Dalbergia Sisoo* from local carpentry was found to be the good adsorbent with large active surface area of 1376 m^{2}g^{-1} and abundance of mesoporosity having pore size 4.06 nm and pore volume of 1.2 cm^{3}g^{-1}. This was achieved by optimized condition of chemical activation by 85% H_3PO_4 in the ratio 1:1 of precursor to activating agent and carbonization at 400 °C. This motivated us to apply *Dalbergia Sisoo* as a material for supercapacitor electrode. Therefore, activated carbon from agro-waste of *Dalbergia Sisoo* can be considered as a promising electrode materials for supercapacitors in combination with transition metal oxides (RuO_2, MnO_x, Fe_2O_3 etc.) (Gomez and Kalu, 2013), to obtain a hybrid capacitor composed of EDLC and pseudocapacitor.

Among the pseudo-capacitive materials, manganese dioxide (MnO_2) is the most promising one due to its high theoretical specific capacitance (1370 Fg^{-1}), wide potential window, rich reserves, and being environmentally-friendly and cost effectiveness (Gomez and Kalu, 2013). Anchoring MnO_2 on carbon substrates such as activated carbon derived from wood leads to development of intercalation and de-intercalation sites on MnO_2. The redox conversion of Mn between (III) to (IV) oxidation states enhances the capacity by favoring faradaic capacitance (Qu et al., 2015).

The reported mechanism of intercalation is commonly written as (Li et al., 2011).

$$MnO_2 + K^+ + e^- \leftrightarrow MnOOK\ . \quad (1)$$

$$(MnO_2)_{\text{surface}} + K^+ + e^- \leftrightarrow (MnO_2\text{-}\ K^+)_{\text{surface}}. \quad (2)$$

Equation (2) represents the surface adsorption of (K^+) on MnO_2.

In hindsight, MnO_2 has poor conductivity. Therefore, its poor conductivity is overcome by compositing with carbonaceous materials (Ilona et al., 2014) which also enhances electro-active surface area.

In this study, we explored the nano-structured AC prepared from *Dalbergia Sisoo* and a hybrid composite with MnO_2 as a core electrode material for supercapacitor via simple facile mechanical mixing method. Wood dust of *Dalbergia sisoo* was used as a whole alternative green source for electrode fabrication for high performance supercapacitors.

2. Experimental sections

2.1. Chemicals and reagents

In this study, analytical grade chemicals and reagents were used without further treatment. Ortho phosphoric acid (85% H_3PO_4) has been purchased from Fischer Scientific, India

and was used as an activating agent. Carbon black (conductor), polyvinlidine fluoride (PVDF) **[-($C_2H_2F_2$)-]** (binder) and N-Methyl-2-pyrolidone (NMP) **(C_5H_9NO)** (dispersing agent) for the fabrication of electrode were obtained from Sigma-Aldrich (USA), manganese dioxide used for making hybrid composite was obtained from Wako Pure Chemical Industries Ltd. The highly porous, corrosion unaffected and excellent electrical conductor Ni-foam was obtained from PRED MATERIALS, International, USA. Ni-foam was used as electrode substrate and current collector. An electrochemical cell was performed in potassium hydroxide (KOH) electrolyte which was purchased from Ajax Finechem, Thermo Fisher Scientific. Wood-dust and splinters of *Dalbergia sisoo* (Sisau) was collected from indigenous carpentry, Kathmandu, Nepal. Double-distilled water has been used throughout the experiment.

2.2. Preparation of AC

Sawdust dust and splinters of *Dalbergia sisoo* were sun-dried for a few days. Then a few preliminary steps have been done, such as crushing, grinding and sieving. A sieve size of 150 μm was used to get a homogenous particle size of wood dust, which was used as precursor for the preparation of AC through activation followed by carbonization.

The activation and carbonization procedures are already reported in our previous study (Shrestha, 2021). In brief, the mixture of precursor/wood dust and H_3PO_4 in the ratio 1:1 (w/w) was left for overnight at room temperature for proper soaking. This impregnated sample was evaporated to dry at 110 °C for 2 h in an oven followed by carbonization at 400 °C for 3 h under the continuous N_2 flow of 100 $mLmin^{-1}$ in a horizontal electric tubular furnace. The carbonized samples were cooled, washed with hot distilled water, dried at 110 °C, grinded and used for advanced physical and electrochemical characterizations (Shrestha, 2021). It was named as activated carbon **Ds**.

2.3. Preparation of electrode-materials and fabrication of electrodes

At first, Ni-foam was taken and cut into small pieces having a size of 5 cm × 1 cm, which was rectangular in shape. It was then used as electrode substrate.

2.4. Preparation of Ds-electrode-material and fabrication of Ds-electrode

Ds-electrode-material was prepared by grinding a mixture of 8 mg of as prepared Ds powder, 1 mg of carbon black powder and 1 mg of PDVF in a mortar. Then 200 μL NMP solution was added to the mixture in order to disperse PDVF. The mixture was again grinded thoroughly and thus paste of electrode material was prepared. Then about 70 μL of paste was applied on rectangular shaped Ni-foam by covering only 1 cm^2 area of it as shown in Fig. 1.

As fabricated Ds-electrode was dried in an oven at 70 °C for overnight. Then electrical contact of the electrode was made through a cu-wire.

In the similar way, hybrid-composite-electrodes (Ds: MnO_2)-HCEs (1:1, 1:2 and 2:1) and MnO_2-electrode have been prepared. The details of amounts of components used for the fabrication of electrodes are shown in Table. 1.

As fabricated electrodes, namely; Ds-electrode, all three hybrid-composite-electrodes (1:1, 2:1 and 1:2 HCEs) and MnO_2-electrode were then pressed individually at 10 kPa pressure for a minute and soaked overnight in 6 M aqueous KOH solution before electrochemical measurements. In this study, aqueous electrolyte KOH is used, because it has been reported that, such electrolyte can provide a higher ionic concentration and lower resistance. Electrochemical energy storage device like supercapacitors containing aqueous electrolyte may display higher capacitance and more power density than those with organic electrolytes, probably due to higher ionic concentration and smaller ionic radius. In addition, aqueous electrolyte can be prepared and utilized without stringently controlling the preparing processes and conditions (Wang et al., 2012).

2.5. Physical characterization of as prepared activated carbon (Ds)

As already been discussed in our published article (Shrestha, 2021), the as prepared activated carbon (Ds) was characterized by different instrumental techniques such as Thermogravimetric Analysis (TGA) / Differential Scanning Calorimetry (DSC) for pyrolytic behavior of Ds; Fourier Transform Infrared Spectroscopy (FTIR) analysis for surface functionality; X-ray diffraction (XRD) analysis for phase study; Raman scat-

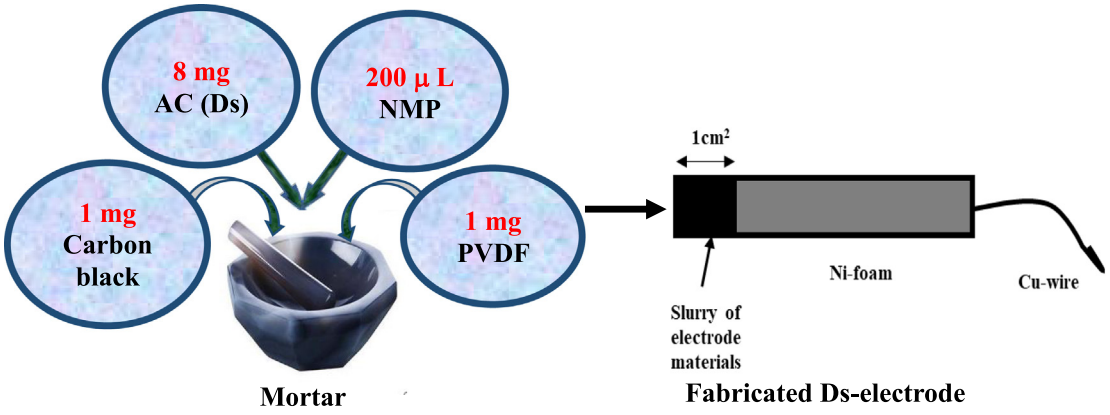

Fig. 1 Fabrication of Ds-electrode.

Table 1 The details of the amount of components for electrodes fabrication.

S.N.	Electrodes	Electrode materials				
		Ds (mg)	MnO_2 (mg)	C-black (mg)	PVDF (mg)	NMP (μL)
1	Ds	8	0	1	1	200
2	1:1 HCE	4	4	1	1	200
3	1:2 HCE	2.66	5.33	1	1	200
4	2:1 HCE	5.33	2.66	1	1	200
5	MnO_2	0	8	1	1	200

tering for identifying defects; Scanning Electron Microscopy (SEM) for surface morphology and Brunauer–Emmett–Teller (BET) for surface area and pore volume analysis. In addition to those techniques, in this paper X-ray Photoelectron Spectroscopy (XPS) was performed for understanding /confirming surface functionality by using a Thermo Fisher scientific, MultiLab 2000 with an Al Kδ source at 1.487 keV at 200 W.

2.6. Electrochemical characterizations

The electrochemical performances of as fabricated Ds-electrode, hybrid-composite-electrodes (HCEs) and MnO_2-electrode were individually tested in electrolyte of 6 M KOH aqueous solution, using 3 electrode experimental set up, consisting of as fabricated Ds-electrode, HCEs and MnO_2-electrode separately as working electrode, Pt-plate as counter electrode and Ag/AgCl as reference electrode. The cell was connected to "Metrohm Autolab (PGSTAT 302 N) potentiostat/galvanostat" system to perform the experiment under room temperature.

For the CV measurement a potential window of −1.0 to −0.2 V was chosen. The varying scan rate of 2, 5, 10, 20, 50 and 100 mV s^{-1} were used. The GCD testing was also observed over the same potential window employing current densities of 1, 2, 3, 5, 10, 15 and 20 Ag^{-1}. From the GCD analysis, cyclic stability (% retention) was estimated. The frequency range of 100 kHz to 0.1 Hz was used at the perturbation signal of 10 mV for the EIS measurement. Nova 1.11 software was used for fitting EIS data (Shrestha and Rajbhandari, 2021).

3. Results and discussion

3.1. Structural analysis of activated carbon (Ds)

As reported in our previous study (Shrestha, 2021), TGA/DSC of the raw wood powder (Ds-R) showed completion of carbonization process at 400 °C. There was only nominal mass change above 400 °C. In TG curve only a slight mass loss was noticed at nearby 100 °C which was due to dehydration. This was proved by a sharp peak of DSC curve at 100 °C. Likewise, in TG curve, an unclear contracted peak was observed at around 200–300 °C, whereas a small mass loss was detected between 200 and 300 °C in DSC curve due to breakdown of hemicellulose which was prominently completed at 300–310 °C. But a prominent mass loss was seen between 300 and 400 °C in TG curves, which were confirmed by a sharp depression at around 390 °C of DSC curve. Therefore it was concluded that cellulose broke down at around 300 °C and all cellulose got converted into organic volatile matters present in raw wood powder. It revealed that, more than 60% of mass got lost around 400 °C (Shrestha, 2021). The precursor material became more stable beyond 400 °C. Therefore 400 °C was considered to be a suitable temperature for carbonization process in this study. FTIR spectra of activated Ds showed the presence of well-defined oxygen containing functional groups such as carboxylic, phenolic, lactonic and ether groups by use of activating agent (H_3PO_4). Oxygen Functional group is an important subject in the study of electrochemical properties of carbon materials- which widely improves-capacitance behavior (Shrestha, 2021).

XRD pattern of activated Ds as reported in previous study (Shrestha, 2021) showed broad peak at around 24 to 26, 2θ degrees from (002) plane and also at around 43 to 45, 2θ degrees from (100) plane indicating the amorphous nature and graphitic crystallites of as prepared activated carbon Ds (Shrestha, 2021). However, the XRD pattern of hybrid composite of Ds:MnO_2 shows the diffraction peaks for β-MnO_2 at 29, 37 and 56°corresponding to (110), (101) and (211) planes. It shows the formation of homogenous composite (Fig. 2).

The amorphous nature of activated Ds was further confirmed by Raman spectrum. The relative intensity ratio of G band to D band was found to be more than 1, which indicates the disordered carbon structure (Shrestha, 2021).

SEM micrographs of as prepared activated carbon Ds at the magnification of x2.0 k, showing well-developed porous morphology is illustrated in Fig. 3. Similar surface morphology was reported in previous publication (Shrestha, 2021).

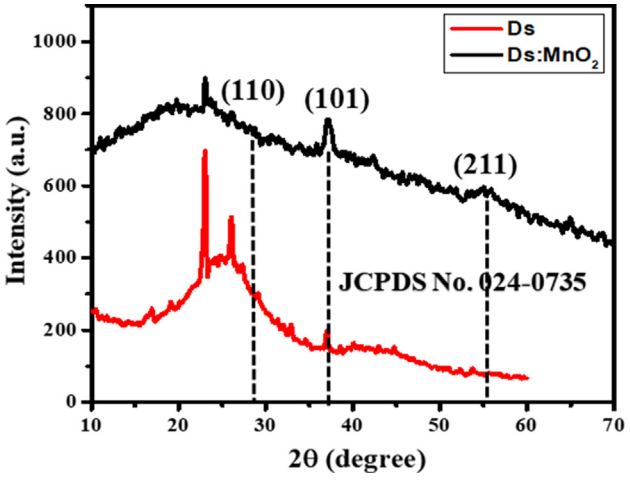

Fig. 2 XRD pattern of Ds and hybrid-composite of Ds:MnO_2.

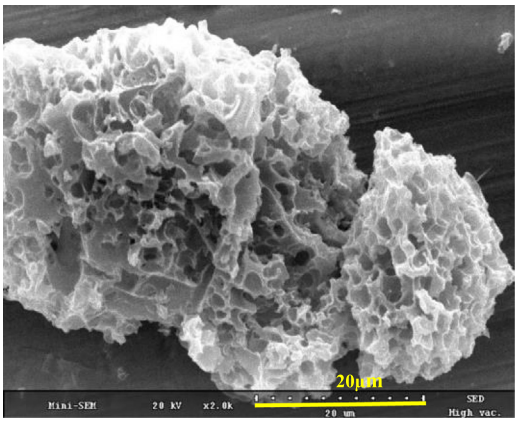

Fig. 3 SEM image of **Ds**.

The BET specific surface area, pore size and pore volume of Ds was found to be 1376 m^2g^{-1}, 4.06 nm and 1.2 cm^3g^{-1}, respectively (Shrestha, 2021). The high specific surface area, small pore size and pore volume make activated Ds a promising material for this study.

3.2. X-ray photoelectron spectroscopy (XPS)

The survey XPS spectrum of activated Ds shows the presence of oxygen, carbon and phosphorus in Ds as shown in Fig. 4**(i)**. The high resolution XPS spectra of C1 s shows a broad peak which was deconvoluted into three peaks at binding energy (BE) 283.3 eV for C-C which is of pure or unfuntionalized carbon, 284.4 eV for ether and alcohol (R-O-R/ –OH) and 287.3 eV for ketone and aldehyde (C = O/ –CHO) as shown in Fig. 4**(ii)** (Pankaj et al., 2018; Kim et al., 2013). Similarly, a broad peak at 532.3 eV for O1s could be seen in Fig. 4**(iii)**, indicating the presence of different chemical states of oxygen. The three deconvoluted peaks for oxygen (O1s) are assigned for phosphatic oxygen (PO_4^{3-}) at 531.2 eV, hydroxyl group (–OH) at 533.0 eV and silicon dioxide (SiO_2) at 533.1 eV. The observation of broad peaks indicate the overlap of various functional groups. From Fig. 4**(ii)** and **(iii)**, it is confirmed that Ds was finely functionalized after an activation with H_3PO_4 and comprises of more acidic functional groups as aldehydes/ketones, ethers, hydroxides (Liang and Xin, 2015). The results revealed that, breakdown of cellulose, hemicellulose and lignin and cross linking of H_3PO_4 as well and functionalization occurred as a consequence after carbonization and activation process (Liang and Xin, 2015). So, it is clear that there is a presence of C and O in activated Ds.

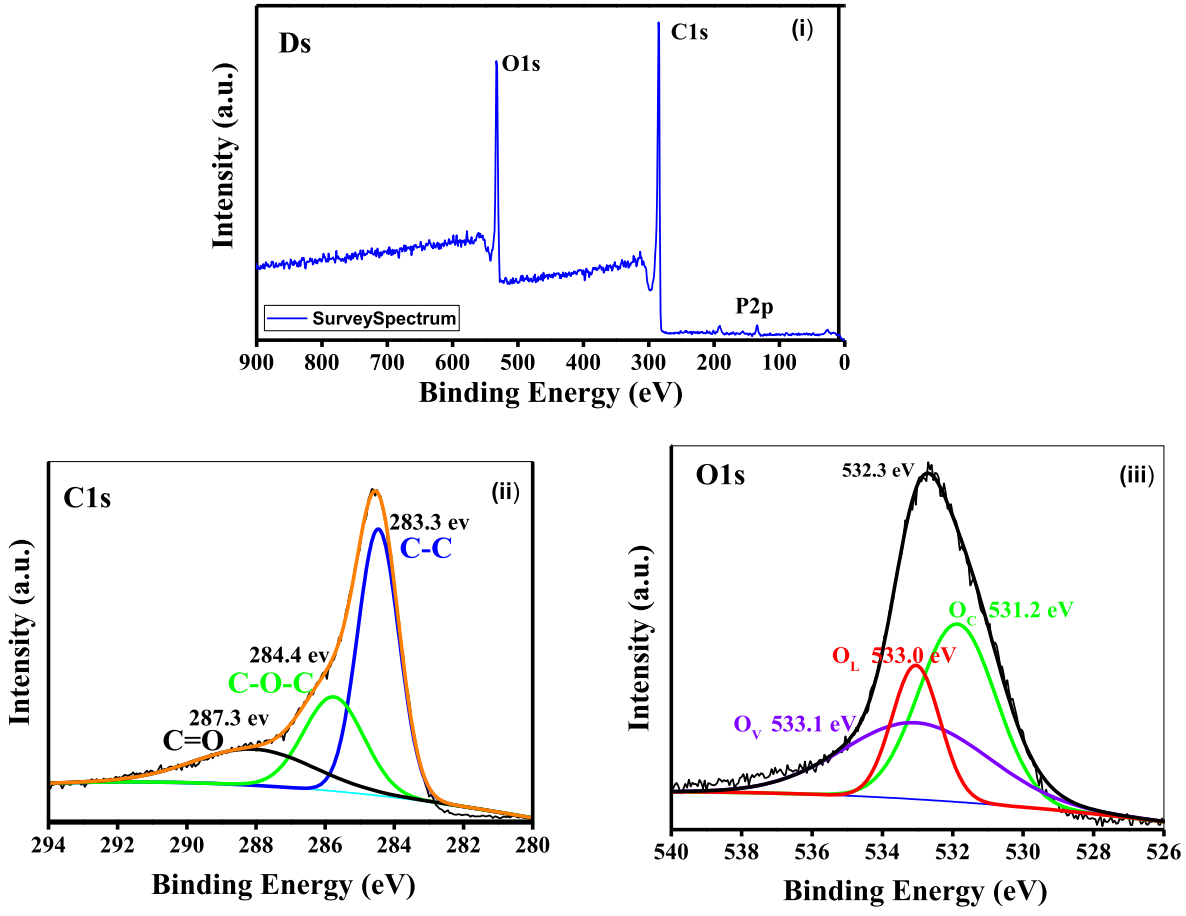

Fig. 4 XPS spectra of Ds.

3.3. Electrochemical characterization for supercapacitor performance

3.3.1. Cyclic voltammetry (CV) study

Fig. 5 shows the cyclic voltammograms of Ds-electrode and its hybrid composite with MnO_2 at different scan rates in 6 M aqueous KOH electrolyte. In the case of Ds-electrode, the curves are not ideal rectangular shape, however there is no redox behavior visible in voltammogram. Therefore, it can be taken as the characteristic of an electrical double layer capacitor (EDLC). Interestingly, the shape of the CV curves was retained even at higher scan rates. This behavior is expected to enable easy and smooth transport of electrolyte ions. Such a mechanism is in agreement with the results of carbonized bio-mass reported by other research groups (Shi et al., 2014; Yu et al., 2011).

But, the addition of MnO_2 has affected both the potential window and voltammogram**.** A potential window of −1.2 to 0 V gave higher current density compared to −1.0 to −0.2 V. The shape of curves was retained in all the three (1:1, 1:2 and 2:1)-HCEs with appearance of redox behavior in the cathodic scan. It was noticeable that an increase in the amount of MnO_2 has resulted in the decrease of current density. This may be due to the large value of bulk resistance of MnO_2 (Puziy et al., 2002). Among all the electrodes, highest current density was observed in 1:1 (Ds:MnO_2)-HCE due to combined effect of high surface area of Ds and optimum resistance and redox behavior of MnO_2.

3.3.2. Galvanostatic charge/discharge (GCD) studies

The electrochemical properties of all the electrodes were further studied using galvanostatic charge/discharge (GCD) process) as shown in Fig. 6.

The potential window for GCD was similar to the one used in CV of respective electrodes. The charge/discharge curves of Ds-electrode are straight line making triangular shape, which confirmed the presence of EDLC behavior. It also hints to the presence of low impurities and proper insertion of electrolyte ions (Gomez and Kalu, 2013) inside the electrode material. From the curve, the specific capacitance ($\mathbf{C_S}$) of Ds-electrode was found to be 104.4 Fg^{-1} at 1 Ag^{-1} using the formula as shown in equation (3),

$$\mathbf{C_S} = \frac{I\Delta t}{m\Delta V} \tag{3}$$

Where, $\mathbf{C_S}$ **(Fg^{-1})** is the specific capacitance (from GCD), **I (A)** is the current, **m(g)** is the mass of sample, **ΔV(V)** is the potential window and **Δt (s)** is the time duration.

Galvanostatic charge/discharge (GCD) response of HCEs, as shown in Fig. 6**b-d,** displayed nearly triangular shape at high current density. However, a bending nature could be observed at current density of 1 and 2 A g^{-1}, which is similar to pseudo-

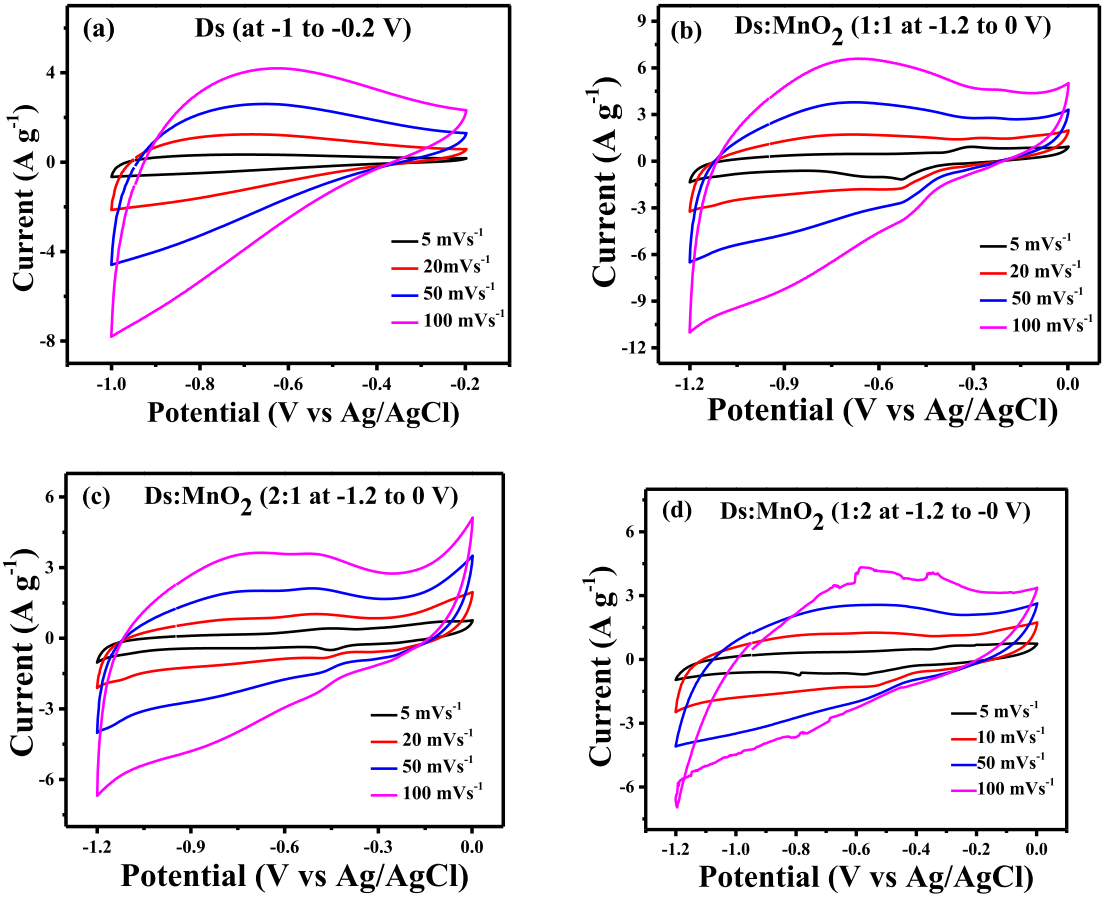

Fig. 5 (a) CV curves of Ds at potential windows (-1 to −0.2 V) and (b), (c) and (d) CV curves of 1:1-(Ds:MnO_2)-HCE, 2:1-(Ds:MnO_2)-HCE and 1:2-(Ds:MnO_2)-HCE at potential windows (−1.2 to 0 V).

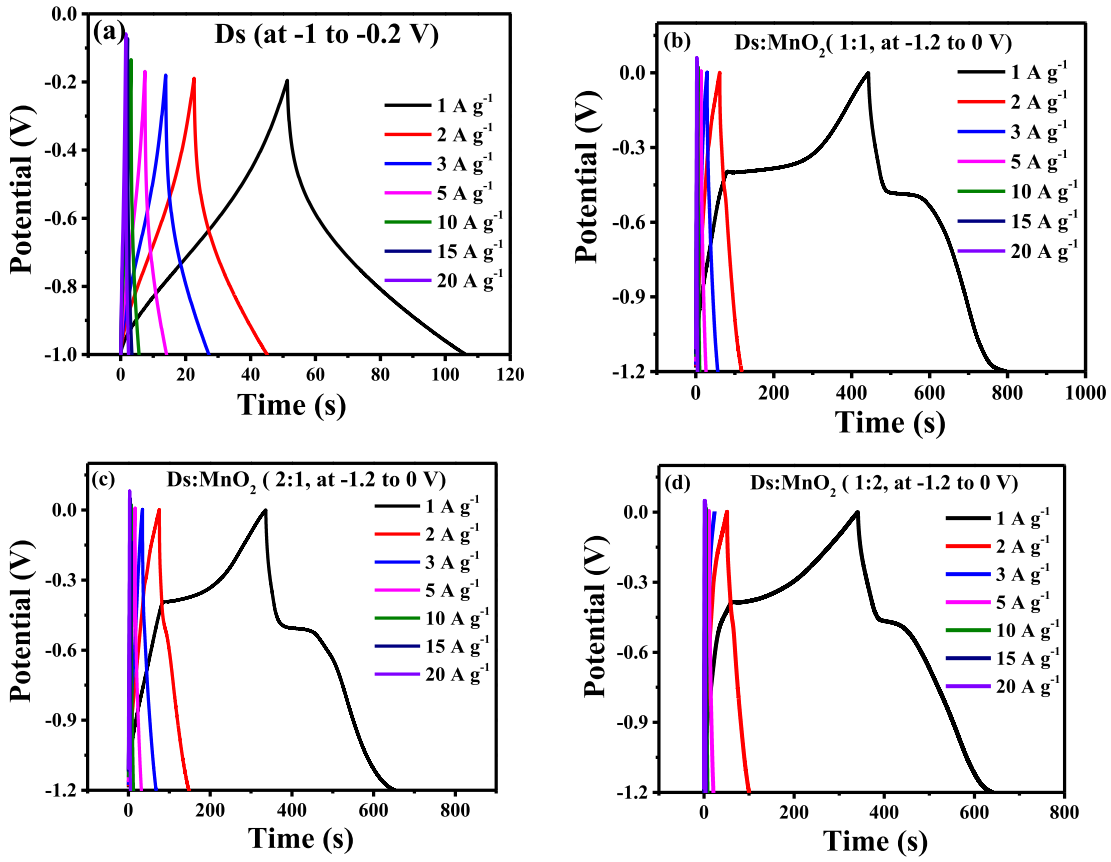

Fig. 6 (a): GCD of Ds-electrode at potential window (-1 to −0.2 V) and (b), (c) and (d): GCD of 1:1-(Ds-MnO_2)-HCE, 2:1-(Ds-MnO_2)-HCE and 1:2-(Ds-MnO_2)-HCE at potential window (−1.2 to 0 V).

Table 2 Specific Capacitance from GCD at different Current Densities.

Current densities ($A\ g^{-1}$)	Specific capacitance (C_S) (Fg^{-1})			
	Ds-electrode	1:1	2:1	1:2
1	104.4	300.1	266.3	250.2
2	80.4	97.5	124.2	83.3
3	71.41	72.1	87.2	59.1
5	62.44	57.3	69.1	45.2
10	51.30	44.4	55.0	33.5
15	46.44	39.5	45.3	30.4
20	42.71	27.4	42.3	28.3

capacitor material (Puziy et al., 2002). It is mainly caused by internal oxidation–reduction reaction occurred in MnO_2. Nevertheless, the curve showed good symmetry, indicating good charge–discharge reversibility of the hybrid composite. The discharge time of 1:1- (Ds:MnO_2)-HCE, 1:2- (Ds:MnO_2)-HCE and 2:1-(Ds:MnO_2)-HCE was found to be about 450 s, 350 s and 330 s, respectively. The specific capacitance calculated was found to be 300.1 Fg^{-1}, 266.3 Fg^{-1} and 250.2 Fg^{-1} for 1:1, 1:2 and 2:1-(Ds:MnO_2)-HCEs, respectively (Shrestha, 2021), which are tabulated in Table 2**.** These values are also compared with the value of Ds-electrode and pure MnO_2-electrode. Among all the electrodes, 1:1-(Ds:MnO_2)-HCE showed best specific capacitance. It may be due to equivalent mixture of Ds and MnO_2, where non-faradaic and faradaic mechanism i.e. EDLC and redox behavior displayed well. The result clearly showed that the equivalent amount of MnO_2 has improved the specific capacitance of 1:1-(Ds:MnO_2)-HCE via simultaneous EDLC and pseudocapacitive charge storage mechanism. Whereas in 1:2, when MnO_2 concentration was increased in the electrode, capacitive performances was decreased and deteriorated the specific capacitance value (266.3 Fg^{-1}) (Shrestha et al., 2019; Shrestha, 2021; Shrestha and Rajbhandari, 2021), which might be due to aggregation of MnO_2 particle within the composite leading to higher value of bulk resistance. Similarly, in 2:1, due to less amount of MnO_2, pseudocapacitive (redox) behavior might be dominated by EDLC behavior generated by Ds, which has led to somewhat lower specific capacitance value (250.2 Fg^{-1}). This is fur-

ther supported by low resistance observed in 1:1-(Ds:MnO_2)-HCE which have also been discussed clearly in EIS analysis section. Here, the specific capacitance (C_S) was calculated using the equation (3).

3.3.3. Effect of current density on the specific capacitance

The Effect of current density on the specific capacitance is presented in Fig. 7. The curve showed that there was a sharp decline of specific capacitance with current density up to 5 A g^{-1} in HCEs. Thereafter, specific capacitance was found to be approximately constant. The decrease in the specific capacitance with increasing current density could be due to the diffusion limited process. At higher current density, the electrolyte ions do not get sufficient time for the diffusion into the inner pores and thus provides lower capacitance (Shi et al., 2014). The specific capacitance of HCEs at different current densities are tabulated in Table 2.

3.3.4. Capacity retention (%)/Life cycle assessment

The life cycle or stability of the as fabricated electrodes was investigated by capacity retention (%). In this study, 1000 continuous charge/discharge cycle was applied at a current density of 3 A g^{-1}. The comparison of capacity retention (%) of Ds-electrode, (Ds:MnO_2)-HCEs and MnO_2 electrode are shown in Fig. 8.

As can be seen in Fig. 8, the capacity retention (%) of Ds-electrode remains high of 82.4% and sustained (1000) prolonged cycles without noteworthy degradation. This revealed that, Ds-electrode has good cyclic stability and it is well fitted for supercapacitor application.

However, the advantage of compositing Ds-electrode with MnO_2 in 1:1 ratio is obvious from its high capacity retention value of 96.3%. In contrary, other two compositions (2:1 and 1:2 Ds:MnO_2-HCEs) show poor retention capacity. This can be explained by poor retention capacity of pure MnO_2-electrode exhibiting only 61% retention capacity at the end of 1000 charge/discharge cycles. It is seen that MnO_2 gets stabilized after 100 cycles presumably due to agglomeration of nanoparticles of MnO_2.

The effect of ESR values on capacity retention was obvious. The best retention capacity of 1:1 Ds:MnO_2-HCEs indicates good electrochemical stability due to excellent electrical conductivity and low degradation of composite (Shrestha et al., 2019; Shrestha, 2021; Shrestha and Rajbhandari, 2021). It is assumed that cycling of potential leads to degradation of active materials, presumably increasing the ESR value and decreasing the % retention capacity in the case of 1:2 and 2:1 composites (Yeung et al., 2015).

3.3.5. Electrochemical impedance spectroscopy (EIS) analysis

Electrochemical Impedance Spectroscopy (EIS) of Ds-electrode, (Ds:MnO_2)-HCEs and pure MnO_2-electrode were performed to investigate the resistive component involved in electrochemical system. Fig. 9 represents the Nyquist plot of EIS measurements of electrodes. In the plot, the vertical axis is imaginary component of the impedance and horizontal axis is the real component.

In Fig. 9, the points are the experimental data. A semi-circle loop at high frequency region is due to total equivalent series resistance (ESR) including electrode and electrolyte and a linear line at low frequency region is due to diffusion and transportation of electrolyte in porous site of electrodes.

Nyquist plot clearly shows the influence of ratios of composite materials on ESR values. The compositing of Ds-electrode has increased the ESR value marginally. Among the hybrid composites, the 1:1 composition has the least ESR value of 0.41 **Ω** while 1:2 composition shows highest ESR value of 0.62 **Ω.** Whereas, the ESR value of MnO_2-electrode was abnormally high (0.72 **Ω**), which are clearly shown in Fig. 9**.** The value of ESR of hybrid composite is obviously affected by the amount of MnO_2. Therefore, composition of the electrode is an important factor in developing the resisting component of the electrode.

3.3.6. Power and energy densities of Ds-electrode

Fig. 10 shows the well-known Ragone plot determined from galvanostatic charge–discharge measurements. Ragone plot of Ds-electrode, 1:1, 1:2 and 2:1 (Ds:MnO_2)-HCE, and pure

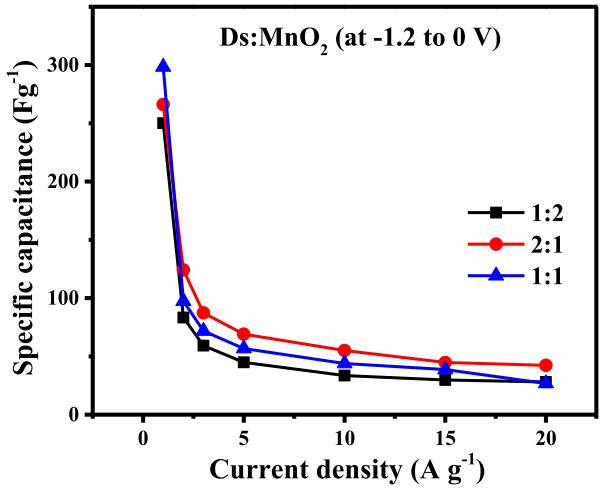

Fig. 7 Specific capacitance of (Ds:MnO_2)-HCEs as a function of current density.

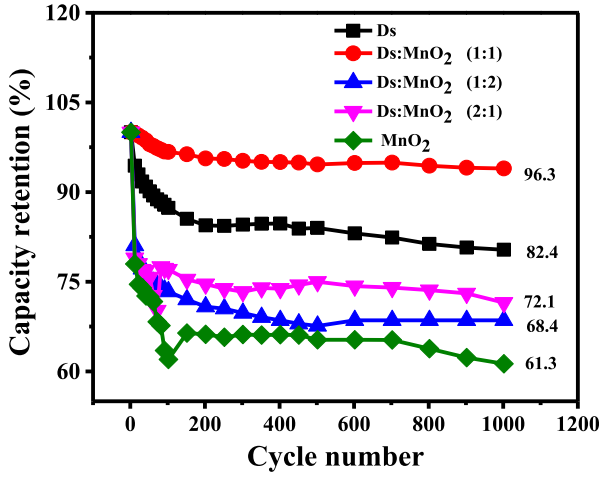

Fig. 8 Capacity retention (%) of Ds-electrode, (Ds:MnO_2)-HCEs and MnO_2 electrode.

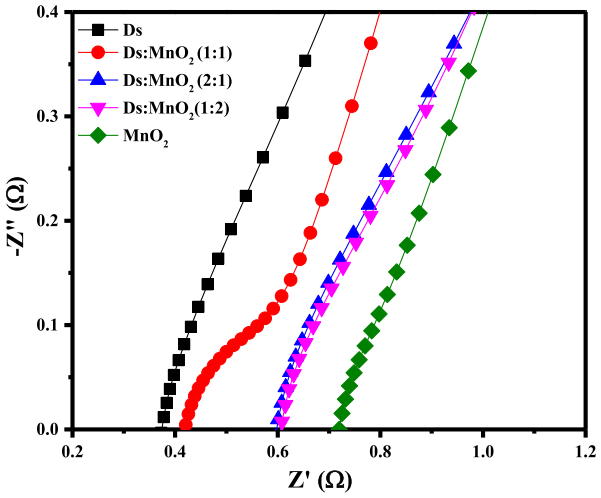

Fig. 9 Nyquist plot of Ds-electrode, (Ds:MnO_2)-HCEs and MnO_2- electrode at frequency range of 100 KHz to 0.1 Hz at the perturbation signal with 10 mV AC voltage in 6 M KOH aqueous solution.

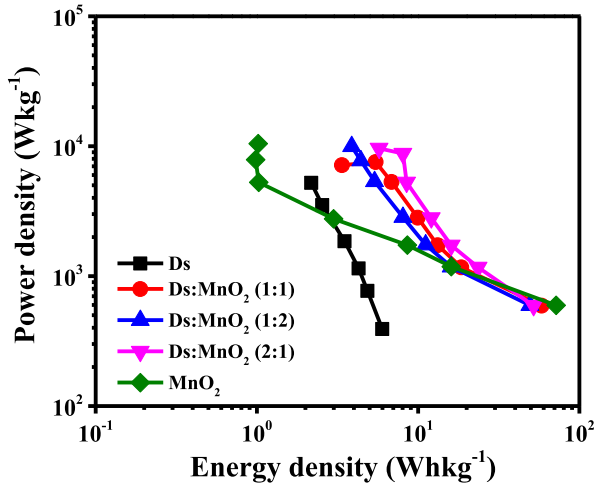

Fig. 10 Ragone plots of Ds–electrode, (Ds:MnO_2)-HCEs in three ratios, and MnO_2-electrode.

MnO_2-electrode at potential window range of (-1.2 to 0 V) are shown in Fig. 10.

The Energy density and Power density plotted in Fig. 10 were calculated by using the formulas as shown in equation (4) and (5),

$$\mathbf{E} = \frac{1}{8} C_{SP} \Delta v^2. \quad (4)$$

$$\mathbf{P} = \frac{E}{\Delta t} \quad (5)$$

where, E is the energy density in W h kg^{-1}, P is the power density in W kg^{-1}, C_{sp} is the specific capacitance in F g^{-1}, ΔV is the potential window (V), whereas Δt (s) is the time of discharge. Since, in this study, three electrode set up was used to measure electrochemical performances, the energy density was obtained by dividing the C_{sp} by 8 instead of 2. The results revealed that Ds-electrode showed the energy density of 2.3 $Whkg^{-1}$ at a power density of 102.2 Wkg^{-1}. Whereas, the energy density of 1:1, 2:1 and 1:2 (Ds:MnO_2)-HCEs were found to be 16.3, 14.4 and 13.2 Wh kg^{-1} at power density of 148.2, 148.5 and 149.0 Wkg^{-1} respectively, which was significantly higher than the value of Ds-electrode (Shrestha et al., 2019; Shrestha, 2021). Similarly, power density was also found to be increased in HCEs than Ds-electrodes. Here, MnO_2 in hybrid composite played the major source of pseudocapacitive characteristics in storing energy. Such type of the mechanisms has also been explained by others (Shrestha et al., 2019; Shrestha, 2021; Lee and Goodenough, 1999). The other reason may be due to the use of higher range of potential window in hybrid composite compared to Ds-electrode.

The overall results of specific capacitance, energy density, power density, capacity retention (%) and ESR value of (Ds)-electrode, (Ds:MnO_2)-HCEs and MnO_2-electrode are tabulated in Table 3.

It was found that, although all the three HCEs exhibited improved electrochemical performances, however, 1:1 HCE showed prominently higher capacitive value of 300.1 Fg^{-1}, which is about three times higher than as fabricated Ds-electrode and energy density 16.3 Wh kg^{-1}, which is six times greater than Ds-electrode. Furthermore, the 1:1 HCE exhibited significantly improved cycling stability of 96.3% from that of Ds-electrode (82.4%). This improvement in electrochemical performances of AC prepared from *Dalbergia sisoo* is attributed to the synergistic effect of MnO_2 that contributes significantly to redox capacitive behavior and decreased ESR value of MnO_2. The results show that the wood dust of Dalbergia sisoo, when functionalized carefully, produce a highly effective active material for energy storage. The energy storage capacity and cyclic stability can be enhanced by incorporating equivalent amount of nanostructured MnO_2. The energy density and power density were comparable and higher than those reported in the literatures (Fujiwara et al., 2001; Xie et al., 2017; Xie et al., 2019). In addition, the electrode material was cheaper alternative to expensive synthetic materials.

Table 3 Specific capacitance, energy density, power density, capacity retention and ESR value of (Ds)-electrode, (Ds:MnO_2)-HCEs and MnO_2-electrode.

Ratio of Composite (Ds: MnO_2)	Potential window (V)	Specific capacitance (Fg^{-1})	Energy density ($Whkg^{-1}$)	Power density (Wkg^{-1})	ESR (Ω)
1:0	−1 to 0	105.2	2.3	102.2	0.38
1:1	−1.2 to 0	300.1	16.3	148.2	0.41
2:1	−1.2 to 0	266.3	14.4	148.5	0.60
1:2	−1.2 to 0	250.2	13.2	149.0	0.62
0:1	−1.2 to 0	362.7	72	597	0.72

4. Conclusion

Conclusively, it is seen from the findings that, AC prepared from waste wood dust of *Dalbergia sisoo* (Sisau), via carbonization process followed by activation with H_3PO_4 was successfully used as an electrode material for supercapacitor in combination with MnO_2. The inclusion of MnO_2 in as prepared activated carbon (Ds) in 1:1 ratio results in superior specific capacitance (300.1 Fg^{-1}), energy density (16.3 $Whkg^{-1}$) and power density (148.2 Wkg^{-1}) compared to Ds, 1:2, 2:1 and MnO_2. Therefore, compositing of AC derived from *Dalbergia sisoo* with MnO_2 has improved the electrochemical performances of electrode material due to its synergistic effect by contributing redox capacity. Accordingly, the waste wood dust of *Dalbergia sisoo*, would act as a potential bio-material source for the preparation of high performance electrode material for low cost energy storage devices like supercapacitor.

Declaration of Competing Interest

The author declare that they have no known competing financial interests or personal relationships that could have appeared to influence the work reported in this paper.

Acknowledgements

Author is thankful to Institute of Science and Technology (IOST), Central Department of Chemistry, Tribhuvan University, Kirtipur, Nepal, Patan Multiple Campus, Tribhuvan University, Patan Dhoka, Lalitpur, Global Research Laboratory (GRL), Sun Moon University, South Korea and Advanced Functional Material Physics (AMP) laboratory, Suranaree University of Technology (SUT), Thailand, for their support to carry out this research work.

References

Brousse, T., Toupin, M. R., Dugas, Athouël, L., Crosnier, O., B elanger, D., 2006. Crystalline MnO_2 as possible alternatives to amorphous compounds in electrochemical supercapacitors. J. Electrochem. Soc. 153 (12), A2171–A2180.

Cao, N., Lyu, Q., Li, J., Wang, Y., Yang, B., Szunerits, S., Boukherroub, R., 2017. Facile synthesis of fluorinated polydopamine/chitosan/reduced graphene oxide composite aerogel for efficient oil/water separation. Chem. Eng. J. 326, 17–28.

Cao, Z., Yang, H., Dou, P., Wang, C., Zheng, J., Xu, X., 2016. Synthesis of three dimensional hollow SnO_2@PPy nanotube arrays via template-assisted method and chemical vapor-phase polymerization as high performance anodes for lithium-ion batteries. Electrochim. Acta 209, 700–708.

Chang, W.M., Wang, C.C., Chen, C.Y., 2019. Fabrication of ultrathin carbon nanofibers by centrifuged-electrospinning for application in high-rate supercapacitors. Electrochim. Acta 296, 268–275.

Dai, C., Wan, J., Yang, J., Qu, S., Jin, T., Ma, F., Shao, J., 2018. H_3PO_4 solution hydrothermal carbonization combined with KOH activation to prepare argy wormwood-based porous carbon for high-performance supercapacitors. Appl. Surf. Sci. 444, 105–117.

Fujiwara, A., Ishii, K., Suematsu, H., Kataura, H., Maniwa, Y., Suzuki, S., Achiba, Y., 2001. Gas adsorption in the inside and outside of single-walled carbon nanotubes. Chem. Phys. Lett. 336, 205–211.

Gomez, J., Kalu, E.E., 2013. High-performance binder-free Co–Mn composite oxide supercapacitor electrode. J. Power Sources 230, 218–224.

Gonzalez-Serrano, E., Cordero, T., Rodriguez-Mirasol, J., Cotoruelo, L., Rodriguez, J.J., 2004. Removal of water pollutants with activated carbons prepared from H3PO4 activation of lignin from kraft black liquors. J. Water Res. 38, 3043–3050.

Huang, Y., Shi, Y., Gong, Q., Weng, M., Li, Y., Gan, J., Wang, D., Shao, Y., Zhao, M., Zhuang, D., 2019. Scalable preparation of hierarchical porous activated carbon/graphene composites for high-performance supercapacitors. J. Mater. Chem. A 7, 10058–10066.

Ilona, A., Katarzyna, L., Agnieszka, S., Grzegorz, L., 2014. Carbon-supported manganese dioxide as electrode material for asymmetric electrochemical capacitors. Int. J. Electrochem. Sci. 9, 2518–2534.

Ke, Q., Wang, J., 2016. Graphene-based materials for supercapacitor electrodes—a review. J. Mater. 2, 37–54.

Kim, M., Hwang, Y., Min, K., Kim, J., 2013. Introduction of MnO2 nanoneedles to activated carbon to fabricate high-performance electrodes as electrochemical super capacitors. Electrochem. Acta 113, 322–331.

Kim, M., Hwang, Y., Min, K., Kim, J., 2013. Introduction of MnO_2 nanoneedles to activated carbon to fabricate high-performance electrodes as electrochemical supercapacitors. Electrochem. Acta 113, 322–331.

Lee, H., Goodenough, J.B., 1999. Supercapacitor behavior with KCl electrolyte. J. Solid State Chem. 144, 220–223.

Lee, Y.J., Park, H.W., Park, S., Song, I.K., 2012. Electrochemical properties of Mn-doped activated carbon aerogel as electrode material for supercapacitor. Curr. Appl. Phys. 12, 233–237.

Li, H., Tao, Y., Zheng, X., Luo, J., Kang, F., Cheng, H.M., Yang, Q. H., 2016. Ultra-thick graphene bulk supercapacitor electrodes for compact energy storage. Energy Environ. Sci. 9, 3135–3142.

Li, F., Wang, J., Liu, L., Qu, J., Li, Y., Bandari, V.K., Karnaushenko, D., Becker, C., Faghih, M., Kang, T., Baunack, S., Zhu, M., Zhu, F., Schmidt, O.G., 2019. Self-assembled flexible and integratable 3D microtubular asymmetric supercapacitors. Adv. Sci. 6, 1901051.

Li, X., Xing, W., Zhuo, S., Zhuo, J., Li, F., Qiao, S.Z., Lu, D.Q., 2011. Preparation of capacitor's electrode from sunflower seed shell. Bioresour. Technol. 102, 1118–1123.

Liang, M., Xin, H., 2015. Microwave to terahertz: characterization of carbon-based nanomaterials. IEEE Microw. Mag. 15, 40–51.

Liang, M., Xin, H., 2015. Microwave to terahertz: characterization of carbon-based nanomaterials. IEEE Microw. Mag. 15, 40–51.

Liu, J.H., Xu, X.Y., Yu, J., Hong, J.I., Liu, C., Ouyang, X., Lei, S., Meng, X., Tang, J.N., Chen, D.Z., 2019. Facile construction of 3D porous carbon nanotubes/polypyrrole and reduced graphene oxide on carbon nanotube fiber for high-performance asymmetric supercapacitors. Electrochim. Acta 314, 9–19.

Lufrano, F., Staiti, P., 2010. Mesoporous carbon materials as electrodes for electrochemical supercapacitors. Int. J. Electrochem. Sci. 5, 903–916.

Ndiaye, N.M., Ngom, B.D., Sylla, N.F., Masikhwa, T.M., Madito, M. J., Momodu, D., Ntsoane, T., Manyala, N., 2018. Three dimensional vanadium pentoxide/graphene foam composite as positive electrode for high performance asymmetric electrochemical supercapacitor. J. Colloid Interface Sci. 532, 395–406.

Pankaj, A., Tewari, K., Singh, S., Singh, S.P., 2018. Waste candle shoot derived nitrogen doped carbon dots basedflourescent sensor probe; an efficient and inexpensive route to determine Hg(II) and Fe(III) from water. J. Environ. Chem. Eng. 6 (4), 5561–5569.

Puziy, A.M., Poddubnaya, O.I., Martínez-Alonso, A., Suárez-Garcia, F., Tascon, J.M.D., 2002. Synthetic carbons activated with phosphoric acid; surface chemistry and ion binding properties. Carbon 40 (9), 1493–1505.

Qu, W.H., Xu, Y.Y., Lu, A.H., Zhang, X.Q., Li, W.C., 2015. Converting biowaste corncob residue into high value added porous

carbon for supercapacitor electrodes. Bioresour. Technol. 189, 285–291.
Ren, H., Shi, X., Zhu, J., Zhang, Y., Bi, Y., Zhang, L., 2016. Facile synthesis of N-doped graphene aerogel and its application for organic solvent adsorption. J. Mater. Sci. 51 (13), 6419–6427.
Salinas-Torres, D., Ruiz-Rosas, R., Morallón, E., Cazorla-Amorós, D., 2019. Strategies to enhance the performance of electrochemical capacitors based on carbon materials. Front. Mater. 6, 115.
Sarkar, A., Singh, A.K., Sarkar, D., Khan, G.G., Mandal, K., 2015. Three-dimensional nanoarchitecture of BiFeO3 anchored TiO2 nanotube arrays for electrochemical energy storage and solar energy conversion. J. ACS Sustain. Chem. Eng. 3 (9), 2254–2263.
Seh, Z.W., Kibsgaard, J., Dickens, C.F., Chorkendor, I., Nørskov, J. K., Jaramillo, T.F., 2017. Combining theory and experiment in electrocatalysis: Insights into materials design. Science 355, eaad4998.
Selvakumar, M., Bhat, K., Aggrawal, M., 2010. Nano ZnO-activated carbon composite electrodes for supercapacitors. Physica B 405 (9), 2286–2289.
Shi, K., Ren, M., Zhitomirsky, I., 2014. Activated carbon-coated carbon nanotubes for energy storage in supercapacitors and capacitive water purification. ACS Sust. Chem. Engine. 2, 1289–1298.
Shrestha, D., 2021. Efficiency of wood-dust of Dalbergia sisoo as low-cost adsorbent for Rhodamine-B dye removal. Nanomater. 11, 2217.
Shrestha, D., Rajbhandari, A., 2021. The effects of different activating agents on the physical and electrochemical properties of activated carbon electrodes fabricated from wood-dust of Shorea robusta. Heliyon 7,. https://doi.org/10.1016/j.heliyon.2021.e07917 e07197.
Shrestha, D., Maensiri, S., Wongpratat, U., Lee, S.W., Rajbhandari, A., 2019. Shorea robusta derived activated carbon decorated with manganese dioxide hybrid composite for improved capacitive behaviors. J. Environ. Chem. Eng. 7, 103227.
Sing, S., Verma, N., 2015. Fabrication of Ni nanoparticles-dispersed carbon micro-nanofibers as the electrodes of a microbial fuel cell for bio-energy production. Int. J. Hydrogen Energy 40 (2), 1145–1153.
Sun, Y., Sills, R.B., Hu, X., She, Z.W., Xiao, X., Xu, H., Luo, W., Jin, X., Xin, Y., Li, T., 2015. A bamboo-inspired nanostructure design for flexible, foldable, and twistable energy storage devices. Nano Lett. 15, 3899–3906.
Wang, G., Zhang, L., Zhang, J., 2012. A review of electrode materials for electrochemical supercapacitors. Chem. Soc Rev. 41 (2), 797–828.
Xie, S., Si, L., Cheng, F., Lu, X., 2017. Recent advances for achieving high-performance carbon fiber materials for supercapacitors. ChemElectroChem 5, 571–582.
Xie, Y., Wang, L., Guo, Q., Yin, J., Liu, J., Fan, L., Wu, J., 2018. Preparation of MnO2/porous carbon material with core-shell structure and its application in supercapacitor. J. Mater. Sci. Mater. Electron. 29, 7957–7964.
Xie, Y., Yang, C., Chen, P., Yuan, D., Guo, K., 2019. MnO2-decorated hierarchical porous carbon composites for high-performance asymmetric supercapacitors. J. Power Sources 425, 1–9.
Xie, Z., Zhu, J., Bi, Y., Ren, H., Chen, X., Yu, H., 2020. Nitrogen-doped porous graphene-based aerogels toward efficient heavy metal ion adsorption and supercapacitor applications. Phys. Status Solidi RRL 14 (1), 1900534.
Yaglikci, S., Gokce, Y., Yagmur, E., Aktas, Z., 2020. The performance of sulphur doped activated carbon supercapacitors prepared from waste tea. Environ. Technol. 41, 36–48.
Yang, G., Park, S.J., 2018. Facile hydrothermal synthesis of NiCo2O4-decorated filter carbon as electrodes for high performance asymmetric supercapacitors. Electrochim. Acta 285, 405–414.
Yang, G., Park, M., Park, S.J., 2019. Recent progresses of fabrication and characterization of fibers-reinforced composites: a review. Compos. Commun. 14, 34–42.
Yeung, K.K., Zhang, X., Kwok, S.C.T., Ciucci, F., Yeun, M.M.F., 2015. Enhanced Cycle life of lead-acid battery using graphene as a sulfation suppression additive in negative active material. RSC Adv. 5, 71314–71321.
Yu, J., Gao, X., Cui, Z., Jiao, Y., Zhang, Q., Dong, H., Yu, L., Dong, L., 2019. Facile synthesis of binary transition metal sulfide tubes derived from NiCo-MOF-74 for high-performance supercapacitors. Energy Technol. 7, 1900018.
Yu, G., Hu, L., Liu, N., Wang, H., Vosgueritchian, M., Yang, Y., Cui, Y., Bao, Z., 2011. Enhancing the supercapacitor performance of graphene/MnO_2 nanostructured electrodes by conductive wrapping. J. Nano Lett. 11, 4438–4442.
Zequine, C., Ranaweera, C.K., Wang, Z., Dvornic, P.R., Kahol, P.K., Singh, S., Tripathi, P., Srivastava, O.N., Singh, S., Gupta, B.K., Gupta, G., Gupta, R.K., 2017. High performance flexible supercapacitors obtained via recycled jute: bio-waste to energy storage approach. J. Sci. Rep. 7, 178–190.
Zhang, Z., Wang, L., Li, Y., Wang, Y., Zhang, J., Guan, G., Pan, Z., Zheng, G., Peng, H., 2017. Nitrogen-doped core-sheath carbon nanotube array for highly stretchable supercapacitor. Adv. Energy Mater. 7, 1601814.
Zhao, H.B., Cheng, J.B., Zhu, J.Y., Wang, Y.Z., 2019. Ultralight CoNi/rGO aerogels toward excellent microwave absorption at ultrathin thickness. J. Mater. Chem. C. 7 (2), 441–448.
Zhu, J., Yang, X., Fu, Z., He, J., Wang, C., Wu, W., Zhang, L., 2016. Three-dimensional macroassembly of sandwich-like, hierarchical, porous carbon/graphene nanosheets towards ultralight, superhigh surface area. Multifunctional Aerogels. Chem. Eur. J. 22 (7), 2515–2524.